Iraqi Journal of Physics, 2023 *Vol. 21, No.1, PP. 21-33*

https://doi.org/10.30723/ijp.v21i1.1086

P-ISSN: 2070-4003
E-ISSN: 2664-5548

Evaluation of Resonance Strengths and Reaction Rates of ^{22}Ne (p, γ) ^{23}Na Nuclear Reaction at Thermonuclear Energies

Ahmed Abdul-Razzaq Selman[1a*]
[1]*Department of Astronomy and Space, College of Science, University of Baghdad, Baghdad, Iraq*
[a*]Corresponding E-mail: ahmed.selman@sc.uobaghdad.edu.iq

Abstract

At thermal energies near stellar conditions, nuclear reactions are sensitive to resonance strengths of the nuclear reaction cross-section. In this paper, the resonance strengths of ^{22}Ne$(p,\gamma)^{23}$Na nuclear reaction were evaluated numerically by means of nuclear reaction rate calculations using a written Matlab code, at the energies of interest in stellar nuclear reactions. The results were compared with standard reaction before and after application of statistical analyses, to select the best parameters that made theoretical results as close as possible to the standard values. Fitting was made for different temperature ranges up to 10 GK, 0.6 GK and 0.25 GK. The evaluated results showed that as the temperature range becomes narrower, more error is added to the evaluated strengths. A proper strength value based on the most recent measured one suggested the difference of at least one order of magnitude can be solved using a numerical evaluation for energies less than 650 keV.

Article Info.

Keywords:
Thermonuclear Physics, Nucleosynthesis, Proton Capture Reactions, p-process in AGB stars, Computational Nuclear Physics.

Article history:
Received: Dec.11, 2022
Accepted: Jan. 29, 2023
Published: Mar.01,2023

1. Introduction

Many physical effects, such as reaction cross-section resonances, highly alter the reaction cross-section for ^{22}Ne$(p,\gamma)^{23}$Na nuclear reaction at low energies. This reaction has an important task in the universe where it provides many nucleosyntheses' reaction benches responsible for producing elements heavier than iron, especially in massive Asymptotic Giant Branch (AGB) stars.

Proton-induced thermonuclear reactions have a unique importance in the universe since they are largely responsible for the so called proton-processes (p-process) in stars. This process is thought to be one of the main reasons behind the continuous generation of heavier elements from lighter ones, especially in large stars. One of these stars, the AGB stars, contributes significantly to the nucleosynthesis of chemical elements of the universe. These stars represent the final phase of nuclear fuel burning at stars with masses less than ~ 10 solar masses, moving in the horizontal branch in the Hertzsprung-Russel Diagram. Although AGB stars share some properties with Red Giant Branch (RGB) stars, usually, these two types have quite different evolutionary paths. AGB stars have their own features due to the mechanism by which nuclear burning occurs at their cores and near-core shells. Mainly, the process involves light elements burning, such as hydrogen and helium, in the layers above the carbon-oxygen core. For some stages in the more massive AGB stars, nuclear burning occurs near to the core with heavier elements [1]. In this case, the AGB stars might undergo through the Hot Bottom Burning (HBB) phase. Furthermore, in the Galactic Center, AGB stars with HBB phase have an essential fingerprint of the abundance of important elements, such as oxygen and sodium isotopes [2]. This is because stars in the HBB phase usually lay between thermally pulsating stages when the AGB stars go through extreme helium-burning reactions. It is thought that the reaction ^{22}Ne$(p,\gamma)^{23}$Na produces a significant amount of sodium in this specific situation through radiative proton capture [3]. This reaction also competes in consuming the available proton particles with another reaction,

namely $^{12}\mathrm{C}(p,\gamma)^{13}\mathrm{N}$.

These reaction's mechanisms highly affect the overall production rates of intermediate elements at galactic centers, especially since the radiative proton capture on ^{22}Ne can alter the ratio of this isotope regarding the other common neon isotopes, namely, ^{21}Ne and ^{20}Ne [3]. Also, there is the observational discrepancy of stars' chemical composition at galactic centers about oxygen and sodium as reported by Cavanna et al. [4].

Introducing the reaction kinematics is a key factor in determining the mechanism of such reactions. The kinematics of the $^{22}\mathrm{Ne}(p,\gamma)^{23}\mathrm{Na}$ reaction has been studied previously through experimental measurements made by Depalo et al. [5] at resonance energies below 1279 keV. Such measurements were highly improved by Kelly et al. [6], which led to a better estimation of the reaction rates of proton capture by ^{22}Ne isotope within 18% [6]. Recently, Lennarz et al. [7] have reported the first inverse kinematic measurement for the reaction $^{22}\mathrm{Ne}(p,\gamma)^{23}\mathrm{Na}$ at low resonance energies. It was shown that important corrections could improve the overall estimation of the elements' abundences in AGB stars. Williams et al. also stated that ^{23}Na isotope availability in cosmological sites with a wealth of AGB stars is minimized by at least a factor of 4 due to this important finding.

However, to evaluate the kinematics of a radiative type of nuclear reaction, one needs to carefully determine the reaction energy yield (or *Q*-value) and the bombardment energy (E_{a}). Doppler shift (ΔE_D) and recoil shift (ΔE_R) parameters, although they depend to some extent on the *Q*-value of the reaction, both have a small contribution to the total reaction kinematics. Thus, these quantities should be considered for a careful analysis [8].

Thermonuclear burning processes may continue in AGB stars to elements with high atomic mass. One of these reactions is the sodium cycle, where the reaction $^{22}\mathrm{Ne}(p,\gamma)^{23}\mathrm{Na}$ plays an important part. The physical quantity that determines the continuity of such reactions to high chains is the mass of the star; thus it is important to consider at which rate this reaction occurs in AGB stars. This reaction involves proton capture at rates depending on the reaction cross-section with ^{22}Ne nucleus, an isotope that also has few roles in the slow neutron capture (the s-process), as well as alpha particle capture in intermediate-mass AGB stars [9]. Therefore, the neon isotope ^{22}Ne enters a few important nuclear reactions in the universe. In $^{22}\mathrm{Ne}(p,\gamma)^{23}\mathrm{Na}$ reaction, there are a few uncertian resonances of narrow widths, which may highly affect the resultant nuclear reaction rate [10], and such nuclear resonances have been resolved with high accuracy recently [11]. Therefore, nuclear reaction rates at low resonance energies give a sharp indication about the validity of nuclear resonance strengths in these important regions.

The aim of this research is to evaluate the reaction kinematics for $^{22}\mathrm{Ne}(p,\gamma)^{23}\mathrm{Na}$ reactions at thermonuclear energies. The current focus is on this reaction due to its importance in stellar evolution, especially in the AGB stars that have a mass range of around 4 solar masses (M_{sun}). The evaluation process in this research was made by including the nuclear resonance strengths at low energies taken from the recent proton capture experiments of ^{22}Ne isotope. These nuclear resonance parameters were used in the calculations of the nuclear reaction rates and were compared with the standard BRUSLIB library [12]. Comparisons were made with the literature to re-estimate the kinematics of the proton radiative capture nuclear reaction by the back substitution and the curve fitting procedures and statistical analysis.

2. Theoretical Concepts

Nuclear resonance strength of any reaction can be described with parameter width of that reaction at a certain energy, $\omega\gamma$, which is the nuclear resonance strength [8]:

$$\omega\gamma = \frac{\omega\Gamma_a\Gamma_b}{\Gamma} \quad (\mathbf{1})$$

Where: Γ_a, Γ_b, and $\Gamma$are the partial widths of reactant particles *a* and *b*, and the total partial width, respectively. The quantity Γ_a can be theoretically found from Breit-Wigner cross-section σ_{WB} at the resonance energy E_r and de Broglie wavelength λ_r as:

$$\Gamma = \frac{\lambda_r^2}{\pi}\frac{\omega\gamma}{\sigma_{WB}} \quad (\mathbf{2})$$

Eq. (2) gives a good description of the nuclear reaction kinematics.

The nuclear reaction rate $\langle\sigma v\rangle$ is an important quantity that is commonly used to describe any nuclear reaction depending on its temperature *T* and other parameters. It can be written in terms of $N_A\langle\sigma v\rangle$, where N_A is Avogadro's number. $\langle\sigma v\rangle$ is the statistical, thermally averaged nuclear cross-section distribution over velocity. Usually, the temperature is converted into 10^9 Kelvins (or Giga Kelvins GK) using T_9 symbol instead of *T*. For a non-resonant nuclear reaction, the reaction rate can be written as:

$$N_A\langle\sigma v\rangle = N_A\left(\frac{8}{\pi\mu}\right)^{\frac{1}{2}}(kT)^{-3/2}\int_0^\infty E\,\sigma(E)\,e^{-E/kT}dE \quad (\mathbf{3})$$

after conversion of unites, Eq (3) becomes [13],

$$N_A\langle\sigma v\rangle \cong \frac{3.732\times10^9}{\left(\mu {T_9}^3\right)^{\frac{1}{2}}}\int_0^\infty E\,\sigma(E)\,e^{-\frac{11.61E}{T_9}}dE \quad \mathrm{cm^3mol^{-1}sec^{-1}} \quad (\mathbf{4})$$

Eq.(3) highly depends on the nuclear excitation energy *E* and the cross-section of the reaction σ, Another practical treatment is to use the Astrophysical Spectroscopic Factor (*S*-Factor) in Eq. (3) instead of the cross section for less dependence of $N_A\langle\sigma v\rangle$ on incident energy *E*. For full details see Ali and Selman [12], and Selman [13]. In Eq. (3), μ is the reduced energy of the reactants, and *k* is Boltzmann's constant. Eq. (3) is modified when considering narrow nuclear resonance peaks at low energies as [8]:

$$N_A\langle\sigma v\rangle = N_A\left(\frac{8}{\pi\mu}\right)^{\frac{1}{2}}(kT)^{-3/2}\int_0^\infty E\,\sigma_{WB}\,e^{-E/kT}dE \quad (\mathbf{5})$$

with the aid of Eqs. (1 and 2), Eq. (5) becomes:

$$N_A\langle\sigma v\rangle = N_A(2\pi)^{\frac{1}{2}}(\mu kT)^{-3/2}\hbar^2\omega\int_0^\infty \frac{\Gamma_a\Gamma_b}{(E_r-E)^2+(\Gamma^2/4)}\,e^{-E/kT}dE \quad (\mathbf{6})$$

thus [8]:

$$N_A\langle\sigma v\rangle = N_A \left(\frac{2\pi}{\mu kT}\right)^{3/2} \hbar^2 \omega\gamma \, e^{-E_r/kT} \quad (7)$$

If there are many narrow nuclear resonances, one can use the summation over Eq. (7) at different strengths $N_A\langle\sigma v\rangle = \sum_{i=1}^{j} N_A\langle\sigma v\rangle_i$, where j is the total number of the narrow resonances that occur at low excitation energies.

An important remark about the $^{22}\mathrm{Ne}(p,\gamma)^{23}\mathrm{Na}$ reaction is that the target nucleus ^{22}Ne contributes also in one of the neutron source reactions, namely $^{22}\mathrm{Ne}(\alpha\,,n)^{25}\mathrm{Mg}$, which provides the neutron seeds for the *s*-process [13].

3. Data and Method

3.1. Data

The goal of this work is to determine the nuclear reaction kinematics from the most recent experimental results for narrow nuclear resonances of $^{22}\mathrm{Ne}(p,\gamma)^{23}\mathrm{Na}$ reactions. A special focus was drawn towards these conditions, especially temperature, which are thought to take place in AGB stars with intermediate masses. The following sections are designated for the nuclear reaction strengths recently published in the literature alongside the comparison with standard libraries for thermonuclear reactions rate values, namely BRUSLIB [10].

The nuclear resonance values used in the present research were taken from the experimental work found in the literature, as listed in Table 1. The experimental statistics of these data are outside the scope of this work. However, during the comparison with standard reaction rate libraries made within this work, it was possible to evaluate these kinematics to a good degree. In intermediate mass AGB stars, the Gamow Window E_G for $^{22}\mathrm{Ne}(p,\gamma)^{23}\mathrm{Na}$ nuclear reaction is between 50 to 600 keV [4], and there are many narrow nuclear resonances in this region. The resonance data for resonance energy E_r with resonances strengths $\omega\gamma$ were taken from Lennarz et al. [3] and Williams et al. [7] and references therein for the reaction $^{22}\mathrm{Ne}(p,\gamma)^{23}\mathrm{Na}$.

It should be mentioned here that only a few examples were found in the literature for other proton reactions on ^{22}Ne isotope, such as $^{22}\mathrm{Ne}(p,n)^{22}\mathrm{Na}$, and $^{22}\mathrm{Ne}(p,\alpha)^{19}\mathrm{F}$ reactions at thermonuclear energies.

In Table 2, the numerical values of reaction rate from BRUSLIB [10] are listed for the reaction $^{22}\mathrm{Ne}(p,\gamma)^{23}\mathrm{Na}$. These data have been directly taken from the website listed in the references, where the temperature T_9 is the temperature T given in GK (1 GK = 10^9 Kelvins), so T_9=1.0 means T=10^9 K; and the reaction rates in cm^3 mol^{-1} sec^{-1}.

3.2. Evaluation Procedure of the Kinematics

The new contribution of this work is to follow a numerical evaluation procedure that uses nuclear resonance strengths at center-of-mass given energies (kinematic) values from Table 1 to find the nuclear reaction rates for the specified case, then compare the results with those from standard libraries. The difference is then statistically weighted to reach the best-evaluated nuclear kinematics. Eq. (7) has been utilized in the present research for this task.

As mentioned in the introduction section, a few discrepancies are found in the literature for resonance strengths of $^{22}\mathrm{Ne}(p,\gamma)^{23}\mathrm{Na}$ nuclear reaction, some of which are a few orders of magnitude. Thus, and to properly evaluate these strengths, a numerical procedure was followed by modifying the formula of Eq. (7) by two multiplication factors, namely f_1 and f_2 as:

Table 1: The nuclear resonance strengths at thermonuclear energies for $^{22}Ne(p,\gamma)^{23}Na$ reaction. Highlighted values are the most recent kinematics.

Reaction	Energy $E_{r(\text{c.m.})}$ (keV)	$\omega\gamma$ (μeV)	Average (or weighted) value of $\omega\gamma$ (μeV)	Ref.
$^{22}\text{Ne}(p,\gamma)^{23}\text{Na}$	1222.0	11.50×10^{6}	11.26×10^{6}	From Lennarz et al. [3] and Williams et al. [7] and references therein.
		11.03×10^{6}		
	632.0	3.2×10^{4}	2.36×10^{5}	
		4.72×10^{5}		
	610.0	2.80×10^{6}	2.50×10^{6}	
		2.45×10^{6}		
		2.44×10^{6}		
	458.0	5.83×10^{5}	5.35×10^{5}	
		5.94×10^{5}		
		4.39×10^{5}		
		4.40×10^{5}		
		4.84×10^{5}		
	248.3	8.20	8.80	
		9.70		
		8.50		
	181.2	2.20	2.45	
		2.70		
		2.32		
		2.17		
	149.4	0.180	0.165	
		0.220		
		0.203		
		0.67		

Table 2: Numerical values of $^{22}Ne(p,\gamma)^{23}Na$ reaction rate from BRUSLIB [10]. T_9 values are given in GK, and $N_A\langle\sigma v\rangle$ are in cm^3 mol^{-1} sec^{-1}.

T_9	$N_A\langle\sigma v\rangle$	T_9	$N_A\langle\sigma v\rangle$	T_9	$N_A\langle\sigma v\rangle$	T_9	$N_A\langle\sigma v\rangle$
0.001	0	0.3	5.4424	1.5	1.3512e+04	7.0	1.5973 e+05
0.005	0	0.4	43.185	2.0	2.6507e+04	8.0	1.7328 e+05
0.010	8.5198e-29	0.5	169.03	2.5	4.2398 e+04	9.0	1.8094 e+05
0.050	1.4693e-09	0.6	447.99	3.0	5.8452 e+04	10.0	1.8187 e+05
0.100	4.9239e-05	0.7	934.41	3.5	7.4362 e+04		
0.150	0.00716	0.8	1663.30	4.0	8.9652 e+04		
0.200	0.15052	0.9	2650.70	5.0	1.1746 e+05		
0.250	1.1993	1.0	3897.30	6.0	1.4097 e+05		

As mentioned in the introduction section, a few discrepancies are found in the literature for resonance strengths of $^{22}\text{Ne}(p,\gamma)^{23}\text{Na}$ nuclear reaction, some of which are a few orders of magnitude. Thus, and to properly evaluate these strengths, a numerical procedure was followed by modifying the formula of Eq. (7) by two multiplication factors, namely f_1 and f_2 as:

$$N_A\langle\sigma v\rangle = f_1 N_A \left(\frac{2\pi}{\mu kT}\right)^{3/2} \hbar^2\, \omega\gamma\, e^{-f_2 E_r/kT} \qquad (9)$$

The numerical parameters f_1 and f_2 are dimensionless fitting parameters. Ideally, f_1 and f_2 should both have values of unity for all kinematics, which means the measured

resonance strengths at a given energy are correct. Any deviation from the unit value of f_1 and f_2 means there should be a difference between measured kinematics and actual ones.

After introducing the concept of resonance, Eq. (7), using the values of Table (1), there was an important inconsistency between the results with the numerical values of Table (2). Hence, this paper attempted to introduce the parameters f_1 and f_2, which are assumed numerically uncorrelated. Suggesting their presence in Eq. (9) is to try to find compensation for the deviation of the values calculated from Eq. (7) and those standard values of Table (2). The f_1 parameter tries to guess the inconsistency of measuring the resonance strength $\omega\gamma$, and f_1 parameter is to determine the possible statistical error presented due to incident energy. These parameters were treated numerically to avoid further complications arising from the Gamow window at low energy reactions of charged particles, the proton in this case.

Eq. (9) can now be fitted to obtain the best numerical values of the parameters f_1 and f_2. For the same data set of $\mu, \omega\gamma,$ and E_r, only T is variable; thus, it was assumed that: $x = T^{-1}$, $y = N_A < \sigma v >, a = f_1 N_A \left(\frac{2\pi}{\mu k}\right)^{3/2} \hbar^2 \omega\gamma,$ and $b = \frac{f_2 E_r}{k}$. a and b are assumed to be constants (fitting parameters). Thus, to evaluate the resonance strengths of the nuclear reaction, one must find the fitting parameters *a* and *b* for the relation:

$$y = ax^m \exp(bx) \qquad (\mathbf{10})$$

Where *m* is any real exponent from $-\infty$ to $+\infty$. This is made straightforward by:

$$\log(a) = \sum_i y_i x_i \; + \frac{3}{2}\sum_i x_{\mathrm{i}} \log(x_i) - b\sum_i x_i \qquad (\mathbf{11}-\boldsymbol{a})$$

$$b = \frac{\left[-\frac{1}{m}\sum_i x_i \; \sum_i y_i \; - \frac{3}{2m}\sum_i \log(x_i)\sum_i x_i \; + \sum_i x_i y_i \; + \frac{3}{2}\sum_i x_i \log(x_i)\right]}{\sum_i x_i^2 \; - \frac{1}{m}\sum_i x_i \log(x_i)} \qquad (\mathbf{11}-\boldsymbol{b})$$

A Matlab main program (*espera.m*) was written to do the kinematics calculations, comparisons, and statistical analysis, including curve fitting of Eq. (10) to calculate the minimal values of the parameters *a* and *b* (hence f_1 and f_2).

It should be noted that if one uses E_{r} and $\omega\gamma$ in units of MeV, masses in amu, and temperature T_9 in GK; then Eq. (7) can be numerically computed as $N_A\langle\sigma v\rangle = [1.54 \times 10^{11}/(\mu T_9)^{3/2}] \times \; \omega\gamma \, e^{-11.605 E_r/T_9}$, and the reaction rate results are in units of $\mathrm{cm}^3\ \mathrm{mol}^{-1}\ \mathrm{sec}^{-1}$. This simplification of units makes curve fitting easier and faster to converge toward minimal error.

Curve fitting analysis using Eqs. (11-*a* and *b*) in this work was made only once for the evaluated values from BRUSLIB. A fitting routine was written and included in the main program to perform the curve fitting using Eq. (10). The fitting range was selected from T_9=0.1 to T_9=0.6 GK, a region assumed to have the most effects of resonances which gives the region of interest or present kinematics. The fitting procedure gave the results of $a = 4.169 \times 10^4$, and $b = 3.202$. The goodness of the fitting was 0.9944, which means the fitting has high confidence.

The simple task now is to back-substitute to calculate the values of f_1 and f_2 for each $\omega\gamma$ and E_{r} values.

3.3. Fitting Goodness

The fitting goodness represents the values of the square of the residuals, or R-Square, which is the deficiency of the ratio between Sum of Square Error SSE to Sum of Square about the mean SST,

$$R - Square = 1 - \frac{SSE}{SST} = 1 - \frac{\sum_i (y_i - y_{e_i})^2}{\sum_i (\bar{y}_i - y_{e_i})^2} \quad (\mathbf{12})$$

Here, $y_i, \bar{y}_i$ and y_{e_i} are theoretical, average-fitted, and fitted values, respectively. The summations are all over the number of points *k*. The goodness of fit therefore varies between 0.0 to 1.0, goodness closer to 1.0 means a better fitting procedure.

The average of SSE is simply the value of SSE over the number of points, *k*, as:

$$Average\ SSE = \frac{SSe}{k} \quad (\mathbf{13})$$

which can also be considered as another criterion for the validity of the fitting procedure while comparing the results.

4. Results and Discussion

In Fig. 1, the results for nuclear resonance energies E_r = 284.3, 458.0, 610.0, and 632.0 keV from Table 1 were plotted as a function of temperature (in GK) for each resonance strength $\omega\gamma$ and were compared with the standard evaluated values taken from BRUSLIB library [10]. Their data are given in Table 2. Calculations were omitted for E_r=149.4 and 181.2 keV due to their large errors. These resonance values are sharp, and since they are found at low energies, they could suffer from a great overlapping between them (see Eq.(1)). Especially for charged-particle nuclear reactions, the Breit-Wigner cross-section at such low nuclear energies comes with uncertainties because the narrow resonance is proportional to the strength, energy and on the shape of cross-section dependence on energy [8]. These points were primarily tested with the present fitting procedure, and it was found that they contribute to a considerable amount of error on the whole curve. Thus, calculations at these energies were ignored for the present purpose.

$\omega\gamma$ values of 2.45×10^6 and 2.44×10^6 μeV for E_r=610 keV were calculated even though they have close values. In Fig. 1, all curves were close together and thus hard to distinguish; for the entire scale, for this reason, only three examples were plotted. In general, the standard results from BRUSLIB were lower than the calculated values by about one order of magnitude. This was also previously reported by Lennarz et al. [3] and Williams et al.Error! Bookmark not defined. Thus it was aimed in this research to seek the best evaluation of resonance strengths for this specific reaction.

4.1. Statistics before Evaluation

To compare with the entire temperature range, a second curve fitting was made for the kinematic values at relatively wide energies (E_r > 200 keV) and compared with experimental values from Table 2. Table 3 shows the results of the second curve fitting, each with the sum of square error and average error. The results of Table 3 were presently calculated and selected based on the error convergence tendency using the relative percentage error, which was used in the sum of square errors SSE. Also, the average of SSE over all data points was calculated and assumed as a measure of goodness for selecting the numerical parameters of f_1 and f_2.

Figs. 2 and 3 show the comparison with BRUSLIB data, and the error analysis for each case is also shown for the same temperature range. So far, the procedure has added

a better match between BRUSLIB and calculated data, as seen from the general improvement between the uncorrected (Fig. 2) and corrected (Fig. 3) data. However, in this case, the used values of f_1 and f_2 are quite large, indicating the improper approach for the entire temperature range. The results at even lower kinematics had more error, and were omitted from Table 3. A general remark about the results of Table 3 is that $\omega\gamma \times f_1 \cong 10^{11}$ cm^3 mol^{-1} sec^{-1}. This indicates that the theoretical values of Eq. (7) are generally accepted and that the error between the standard and calculated values should be minimal, with a very weak dependence on the exponent part. To strengthen this conclusion, data for $\omega\gamma$ vs. f_1 from Table 3 was used in a third curve fitting using the exponential form, $f_1 = c\,\exp(d \times \omega\gamma)$; and the results showed that c = 4.108$\times 10^{10}$and d=-2.358×10^{-4}, with R-Square =1.0, which means the fit was exact. The value of the parameter d (units of MeV^{-1}) explains the slow dependence of f_1 on $\omega\gamma$. This also means that the fitting results listed in Table 3 have a generally good behavior.

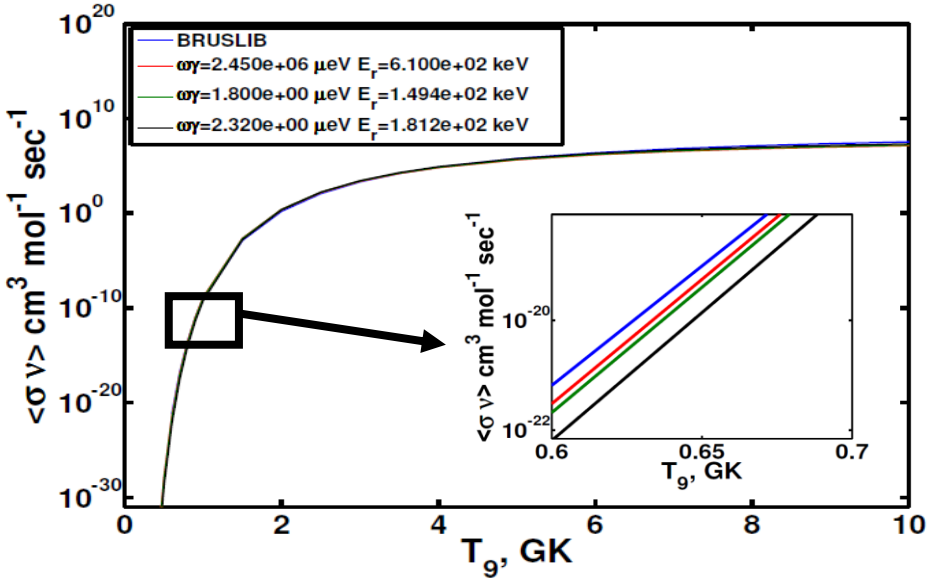

Figure 1: Reaction rates calculated using epera.m code for resonance values of Table 1, plotted with the theoretical values taken from BRUSLIB [10]. Only 3 examples are shown.

There is another important remark seen from Figs. 2 and 3, that is, the error for all curves tends to converge at T_9 between 0.5 and 2.5 GK; and increases before and after this range. This is expected since the resonance strengths act more significantly at the proper temperature for the same incident energy E_r. The final curve is given in Fig. 4, where one can clearly notice that as the temperature increases, the error decreases. Thus, to select the best statistics for the current evaluation, two more curve fittings were also performed for temperature ranges T_9=0.001 – 0.25, and T_9=0.001 – 0.6. The results of this treatment are shown in Figs. 5 and 6.

4.2. Statistics after Evaluation

The same results were found, assuming that the effects of resonances took place in a limited region. These results in the region of interest are given in Table 4. To have a good insight into the evaluation process, the values of this table were calculated for two temperature ranges, T_9=0.001 – 0.6 GK and T_9=0.001 – 0.25 GK. Note that the values of the fitting parameter b from Eq. (11) do not depend on $\omega\gamma$, but it only depends on E_r. The results shown in Table 4 were found from the values obtained from the fitting procedure, a = 4.169 $\times 10^4$, and b = 3.202. The fitting procedure depended on Eq. (10) to describe data from BRUSLIB [10] for $^{22}\mathrm{Ne}(p,\gamma)^{23}\mathrm{Na}$ reaction, and the results are given in Figs. 5 and 6 for both temperature ranges, respectively.

Table 3: Calculated numerical evaluation results of resonance strengths for $^{22}Ne(p,\gamma)^{23}Na$ reaction from present approach. This comparison was made assuming all T_9 range. f_1 and f_2 are dimensionless parameters.

Energy $E_{r(c.m.)}$ (keV)	$\omega\gamma$ (μeV)	f_1	$f_1/931.5^{1.5}$	f_2	SSE	Average SSE	Case no
1222.0	11.50×10^{6}	2.32×10^{4}	0.8160	3.15	4.2321	0.1513	2-a
	11.03×10^{6}	2.34×10^{4}	0.8231	3.25	4.9047	0.1752	2-b
632.0	3.2×10^{4}	2.10×10^{7}	738.66	6.32	9.8820	0.2790	2-c
	4.72×10^{5}	6.22×10^{5}	21.878	5.81	12.7369	0.4549	2-d
610.0	2.80×10^{6}	9.5×10^{4}	3.3416	6.33	3.1495	0.4591	2-e
	2.45×10^{6}	9.49×10^{4}	3.3380	6.38	2.9344	0.3769	2-f
	2.44×10^{6}	9.49×10^{4}	3.3380	6.38	2.8741	0.3813	2-g
458.0	5.83×10^{5}	9.41×10^{5}	33.099	8.62	8.0783	0.2885	3-a
	5.94×10^{5}	9.34×10^{5}	33.169	8.70	4.9910	0.1780	3-b
	4.39×10^{5}	8.41×10^{5}	29.581	8.60	3.5242	0.1260	3-c
	4.40×10^{5}	8.41×10^{5}	29.581	8.60	3.0259	0.1081	3-d
	4.84×10^{5}	9.12×10^{5}	32.079	8.60	7.5711	0.2704	3-e
248.3	8.20	4.10×10^{10}	1.44×10^{6}	15.78	2.8458	0.1016	3-f
	9.70	4.10×10^{10}	1.44×10^{6}	15.80	3.7048	0.1323	3-g
	8.50	4.10×10^{10}	1.44×10^{6}	15.84	2.9276	0.1046	3-h

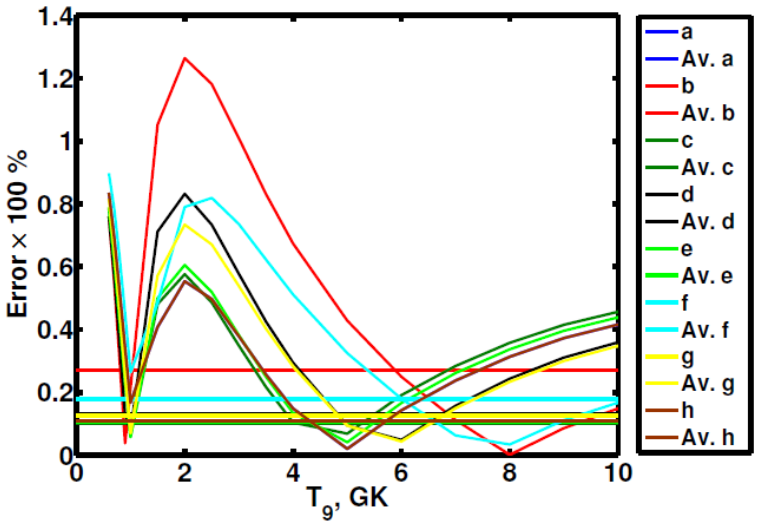

Figure 2: Relative error (curved lines) and average error (straight lines) for the difference between theoretical and calculated reaction rates for all temperature range before applying the correction from the fitting procedure. Theoretical values were taken from BRUSLIB [10]. Shown are the results taken from Table (3) for E_r=1222.0, 632 and 610 keV (cases 2-a to 2-g). Temperature range was T_9=0.001 to 10.

The calculated error and average error for the cases (5-g and 6-g), (5-h to 6-i), and (5-j to 6-k) were almost identical, so they were plotted once for each set. From these figures and Table 4, the behavior is now clearer, and the error of evaluation increased as the temperature range moved away from lower energies and increased if one included high values of T_9.

In this case, the exponential part of Eq. (7) was overly sensitive to small changes even with the inclusion of the factors f_1 and f_2; therefore another correction was needed to reduce the error indicated in the column (factor by f_2) in Table 4. This reduced the fast change during the calculation and improved the goodness of fit. The existence of this parameter strongly suggests that the main difference in the form of Eq. (7) with

standard data results from the inverse dependence on T_9 in the exponent. This conclusion also supports the previous one when treating the entire scale of T_9.

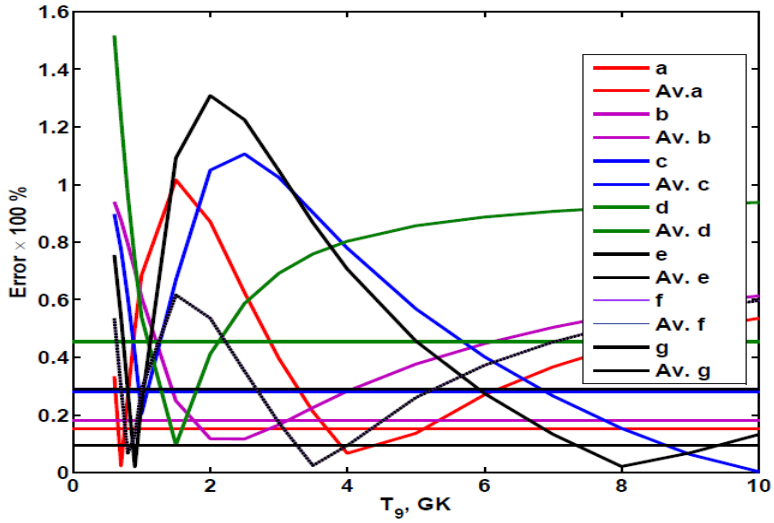

Figure 3: Relative error (curved lines) and average error (straight lines) for the difference between theoretical and calculated reaction rates for all temperature range before applying the correction from the fitting procedure. Theoretical values were taken from BRUSLIB [10]. Shown are the results taken from Table (3) for E_r=458 and 248.3 keV (cases 3-a to 3-h). Temperature range was T_9=0.001 to 10.

From Table 4, the evaluated results showed good behavior for all resonance strengths $\omega\gamma$. At the same E_r, and for the cases when $\omega\gamma$ were close or different, the resultant evaluated strengths were close and at least within the same order of magnitude. Especially for E_r=632.0 keV, the experimental strengths had a whole order of magnitude, while the evaluated results were almost identical at $(\omega\gamma)_{\text{evaluated}} = 25.325\times 10^4$ μeV. A similar note is seen for E_r=610.0 keV and the important resonance at E_r=458.0 keV. However, the procedure still has some descripancy at the first resonance E_r=1222.0 keV. This point is worthy of further investigation.

The results of $\omega\gamma$ (in μeV) in Table (4) are not fitting of resonance strenghth $\omega\gamma$ (μeV), but they are results from the evaluation procedure explained previously in section 3.2.

Finally, from comparing the results of Figs. 5 and 6, the present method worked the best at the temperature range T_9=0.001 – 0.6 since the average error (straight lines) were all close; and confined within the approximate range of (0.65 – 0.75%), as seen in Fig. 5. This remark was not seen in Figs. 2 and 3.

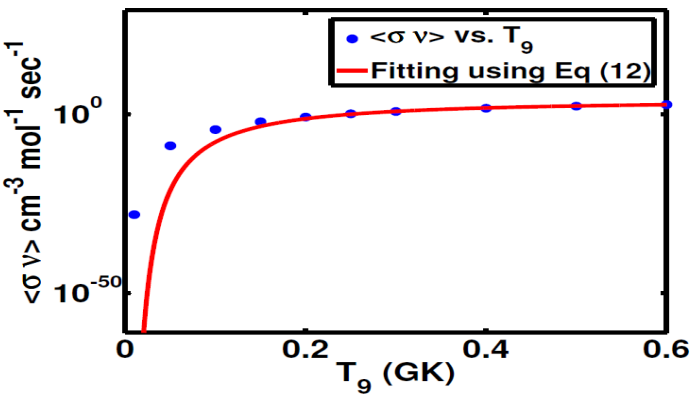

Figure 4: The results of fitting procedure for theoretical reaction rates of $^{22}Ne(p,\gamma)^{23}Na$ nuclear reaction using Eq. (10). The fitting parameters were a = 4.169 × 10^4, and b = 3.202, and the goodness was 0.9944.

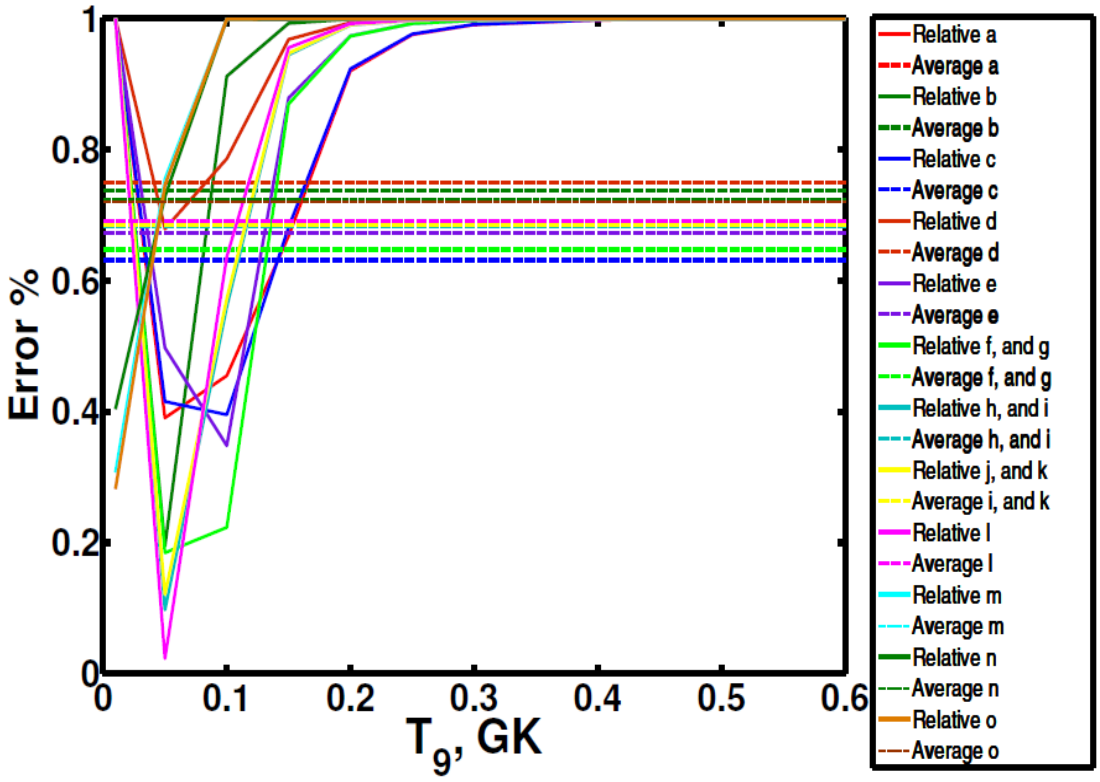

Figure 5: The results of fitting procedure for theoretical reaction rates of $^{22}Ne(p,\gamma)^{23}Na$ nuclear reaction using Eq. (10) for each value in Table (4). These statistics are for temperature range T_9=0.001-0.6.

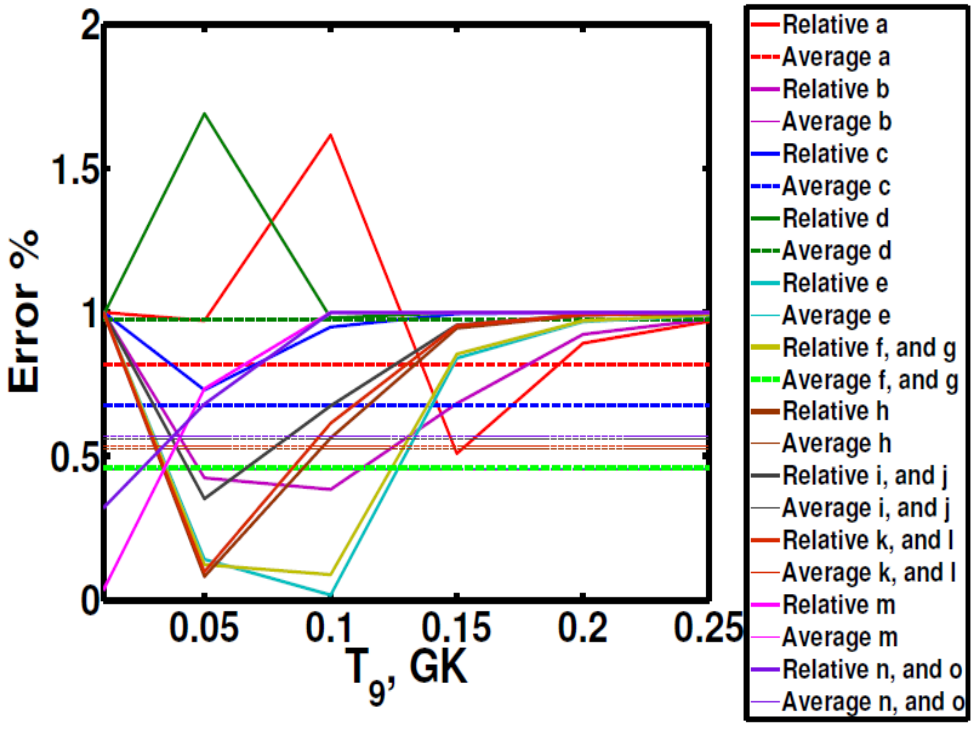

Figure 6: The same as Fig. 5 for the temperature range T_9=0.001-0.25.

Table 4: Numerical evaluation results of resonance strengths for $^{22}Ne(p,\gamma)^{23}Na$ reaction. This comparison was made assuming specific T_9 range 0.001 to 0.6 GK and 0.001 to 0.25 GK. f_1 and f_2 are dimensionless parameters found from the values obtained by fitting procedure, a = 4.169 ×10^4, and b = 3.202 – see Eqs (11-a and b).

$E_{r(c.m.)}$ (keV)	$\omega\gamma$ (μeV)	f_1	f_2	Factor by f_2	T_9 start to T_9 stop GK	SSE	Average SSE	Fig	$\omega\gamma$ evaluated (μeV)
1222.0	11.50×10^6	0.2020	-0.2258	0.3151	0.001-0.6	7.578	0.6315	5-a	2.323×10^6
				0.3001	0.001-0.25	4.878	0.1830	6-a	
	11.03×10^6	.2300		0.3153	0.001-0.6	7.575	0.6313	5-b	2.645×10^6
				0.3020	0.001-0.25	3.725	0.4657	6-b	
632.0	3.2×10^4	7.9141	-0.4366	0.4570	0.001-0.6	8.852	0.7377	5-c	25.325×10^4
				0.4840	0.001-0.25	3.222	0.5360	6-c	
	4.72×10^5	0.5366		0.5462	0.001-0.6	8.999	0.7492	5-d	2.532×10^5
				0.4862	0.001-0.25	9.002	1.1251	6-d	
610.0	2.80×10^6	0.0904	-0.4532	0.6000	0.001-0.6	8.096	0.6721	5-e	0.2531×10^6
				0.5790	0.001-0.25	3.645	0.4556	6-e	
	2.45×10^6	0.1034		0.5842	0.001-0.6	7.765	0.6471	5-f	0.2533×10^6
				0.5760	0.001-0.25	3.680	0.4600	6-f	
	2.44×10^6	0.1038		0.5700	0.001-0.6	3.212	0.2150	5-g	0.2532×10^6
				0.5658	0.001-0.25	2.939	0.7582	6-g	
458.0	5.83×10^5	0.4344	-0.6024	0.7190	0.001-0.6	8.198	0.6824	5-h	2.5325×10^5
				0.7195	0.001-0.25	4.193	0.5241	6-h	
	5.94×10^5	0.4264		0.7195	0.001-0.6	8.260	0.6849	5-i	2.5328×10^5
				0.7195	0.001-0.25	4.185	0.5231	6-i	
	4.39×10^5	0.5769		0.7156	0.001-0.6	8.214	0.6845	5-j	2.5326×10^5
				0.7343	0.001-0.25	4.473	0.5592	6-j	
	4.40×10^5	0.5756		0.7153	0.001-0.6	8.119	0.6214	5-k	2.5326×10^5
				0.7140	0.001-0.25	8.280	0.6380	6-k	
	4.84×10^5	0.5232		0.7110	0.001-0.6	8.297	0.6914	5-l	2.5322×10^5
				0.7100	0.001-0.25	4.275	0.5345	6-l	
248.3	8.20	3.08 × 10^4	-1.1112	0.7180	0.001-0.6	8.663	0.7219	5-m	25.26×10^4
				0.7125	0.001-0.25	4.539	0.5674	6-m	
	9.70	2.61 × 10^4		0.7220	0.001-0.6	8.691	0.7243	5-n	25.317×10^4
				0.7120	0.001-0.25	4.565	0.5706	6-n	
	8.50	2.97 × 10^4		0.7185	0.001-0.6	8.635	0.7195	5-o	25.245×10^4
				0.7160	0.001-0.25	4.568	0.5710	6-o	

5. Conclusions

The present paper used numerical evaluation to refine the resonance strengths $\omega\gamma$ of the nuclear reaction cross-section for the nuclear reaction $^{22}\mathrm{Ne}(p,\gamma)^{23}\mathrm{Na}$ at thermal energies of interest for stellar reactions. From the above results, the procedure showed a generally consistent results for almost all resonance strengths found in the recent literature, except for those at E_r=1222.0 keV. Especially for energy E_r=632.0 keV, the current treatment successfully solved the problem of resonance strength differences based on numerical evaluation, and the evaluated results were $\omega\gamma = 25.325\times 10^4$ μeV.

It was also shown that the best temperature range for the present treatment was at T_9=0.001 – 0.6, where the present evaluation resulted in minimal error at this range compared with the entire (T_9=0.001 – 10) and small (T_9=0.001 – 0.25) ones.

Acknowledgement

The author would like to thank Department of Astronomy and Space, College of Science, University of Baghdad.

Conflict of Interest

There is no conflict of interest in this research.

References

1. A. I. Karakas, G. Cinquegrana, and M. Joyce, M. Noti. Royal Astron. Soc. **509**, 4430 (2022).
2. F. Herwig, Annu. Rev. Astron. Astrophys. **43**, 435 (2005).
3. A. Lennarz, M. Williams, A. Laird, U. Battino, A. Chen, D. Connolly, B. Davids, N. Esker, R. Garg, and M. Gay, Phys. Lett. B **807**, 135539 (2020).
4. F. Cavanna and P. Colombetti, in J. Phys.: Conference Series (IOP Publishing, 2020). p. 012045.
5. R. Depalo, F. Cavanna, F. Ferraro, A. Slemer, T. Al-Abdullah, S. Akhmadaliev, M. Anders, D. Bemmerer, Z. Elekes, and G. Mattei, Phys. Rev. C **92**, 045807 (2015).
6. K. Kelly, A. Champagne, L. Downen, J. Dermigny, S. Hunt, C. Iliadis, and A. Cooper, Phys. Rev. C **95**, 015806 (2017).
7. M. Williams, A. Lennarz, A. Laird, U. Battino, D. Connolly, C. Ruiz, A. Chen, B. Davids, and N. Esker, Phys. Rev. C **102**, 035801 (2020).
8. C. Iliadis, *Nuclear Physics of Stars* (John Wiley & Sons, 2015).
9. A. A. Selman, NeuroQuantology **20**, 5953 (2022).
10. S. Goriely. *BRUSLIB: The Brussels Nuclear Library for Astrophysics Applications*; www.astro.ulb.ac.be/bruslib/index.html.
11. A. A. Selman, Iraqi J. Sci. **64**, 984 (2023).
12. L. T. Ali and A. A. Selman, Iraqi J. Sci. **62**, 1734 (2021).
13. L. T. Ali and A. A. Selman, in J. Phys.: Conference Series (IOP Publishing, 2021), p. 012110.

تقييم شدات الرنين ومعدلات التفاعل النووي ^{22}Ne(*p, gamma*)^{23}Na عند الطاقات النووية الحرارية

أحمد عبد الرزاق سلمان[1]

[1] قسم الفلك والفضاء، كلية العلوم، جامعة بغداد، بغداد، العراق

الخلاصة

في الطاقات الحرارية بالقرب من الظروف النجمية، تكون التفاعلات النووية حساسة لشدة الرنين في مساحة المقطع العرضي للتفاعل النووي. في هذا البحث تم تقييم قوة الرنين للتفاعل النووي $^{22}\mathrm{Ne}(p,\gamma)^{23}\mathrm{Na}$ عدديًا عن طريق حسابات معدل التفاعل النووي باستخدام برنامج كتب بلغة البرمجة (ماتلاب Matlab) عند طاقات ذات الأهمية في التفاعلات النجمية النووية. وتمت مقارنة النتائج مع قيم التفاعل القياسية قبل وبعد تطبيق التحليل الإحصائي لاختيار أفضل المعلمات التي تعطي نتائج نظرية أقرب ما يمكن من القيم القياسية. تم إجراء عدة عمليات ملائمة في درجات حرارة مختلفة تصل إلى 10مليار كلفن و 0.6 مليار كلفن و 0.25 مليار كلفن، وقد أظهرت النتائج المقيمة أنه عندما يصبح نطاق درجة الحرارة أضيق، يضاف المزيد من الخطأ إلى نقاط القوة المقيمة. وتشير قيمة شدات الرنين المستندة إلى أحدث قياس تم نشره سابقا إلى وجود اختلاف بمقدار مرتبة واحدة على الأقل، وقد تم تقييم تلك الشدات بنجاح عند طاقات اقل من 650 كيلو الكترون فولط.